Strong hydrogen-related electronic effects on the shear elastic constant of $TaV_2H(D)_x$

K. Foster, J. E. Hightower, and R. G. Leisure
Department of Physics, Colorado State University, Fort Collins, Colorado 80523-1875

A. V. Skripov
Institute of Metal Physics, Urals Branch of the Academy of Sciences, Ekaterinburg 620219, Russia
(Received 13 August 2001; published 11 February 2002)

Resonant ultrasound spectroscopy has been used to measure the shear modulus of the $C15$ Laves-phase compounds $TaV_2H(D)_x$. Polycrystalline samples with $x(H)=0.00$, 0.06, 0.10, 0.18, 0.34, and 0.53 and $x(D)=0.17$ were investigated. Measurements were made over a temperature range of 3–345 K. Both the temperature dependence and the magnitude of the shear modulus $[G(T)]$ were found to be highly dependent on the hydrogen concentration (x). At 20 K, $G(T)$ for $TaV_2H_{0.53}$ was 55% greater than that of TaV_2. For H concentrations of $x \leqslant 0.10$, $G(T)$ of TaV_2H_x shows anomalous stiffening with increasing temperature almost across the entire temperature range of study. For H concentrations $x \geqslant 0.18$ the temperature dependence of $G(T)$ was reversed compared to that of the lower concentrations, exhibiting a more normal softening with increasing temperature. A minimum was found in $G(T)$ for $TaV_2H_{0.10}$ and $TaV_2H_{0.18}$ at approximately 40 and 300 K, respectively. The results are in agreement with a model detailing electronic contributions to the single-crystal elastic constant c_{44}. The symmetry of the $C15$ structure results in doubly degenerate electronic energy levels at the X point of the Brillouin zone. These levels couple to an e_4 strain with resulting effects on c_{44}. The experimental results imply that the Fermi level of TaV_2 lies very close to the double-degeneracy point. The effect of hydrogen is to raise the Fermi level above the double-degeneracy point with a resulting large change in the electronic contribution to c_{44}, which in turn affects the polycrystalline modulus $G(T)$. The shift of the Fermi level with increasing hydrogen concentration determined from the elastic constant measurements is in remarkable agreement with the shift calculated from the electronic density of states available from other experiments. The results imply that each hydrogen atom contributes approximately one electron at the Fermi energy.

DOI: 10.1103/PhysRevB.65.094108 PACS number(s): 62.40.+i, 62.80.+f, 71.90.+q, 74.70.Ad

I. INTRODUCTION

The second-order elastic constants of materials are given by the second derivative of a thermodynamic potential with respect to strain. For adiabatic elastic constants the appropriate potential is the internal energy, while for isothermal elastic constants it is the Helmholtz free energy.[1,2] (Ultrasonic measurements give the adiabatic, i.e., constant entropy, elastic constants because there is essentially no exchange of heat between different parts of the sample during a vibration period. The difference between the adiabatic and isothermal modulus is usually a few percent at most.) The elastic constants are of both practical and fundamental interest. For engineering applications the elastic constants are used to calculate parameters such as the fracture toughness, thermoelastic stress, and elastic instabilities.[3] The elastic constants can be used to calculate basic parameters of materials including the bulk modulus (B), Young's modulus (E), shear modulus (G), Poisson's ratio (ν), and sound velocities. The elastic constants relate to a variety of phenomena in condensed matter physics, such as interatomic potentials, equations of state, and phonon spectra. Through the Debye theory they are also related to the thermal properties of solids such as specific heat, Debye temperature, and thermal expansion.

The temperature (T) dependence of the elastic constants is directly related to the anharmonic nature of lattice vibrations. The lattice vibrations typically result in a T^4 term at low temperatures and a term linear in temperature at higher temperatures.[4] In metals there is also a contribution from the conduction electrons. For simple metals the electrons contribute a T^2 term at low temperatures.[5] Volume effects, through the thermal expansion of the crystalline lattice, play a significant role. The overall result, for typical materials, is that the elastic moduli approach 0 K with zero slope and decrease monotonically with increasing temperature. This simple picture is not applicable to materials undergoing phase transitions[6,7] or to materials with more complicated electronic structures.[8]

The elastic constants of the Laves-phase compounds have been the subject of a large number of theoretical[9–11] and experimental investigations.[12–18] There is a vast number of binary (AB_2) Laves-phase intermetallic compounds[19] which form with three different symmetries: the $C15$ cubic, the $C14$ hexagonal, and the $C36$ structures. The elastic properties of the Laves phases have created interest for a variety of reasons. First, the Laves-phase alloys form the largest single group in the topologically close-packed (TCP) set of materials. The TCP materials[20] have relatively low densities and high melting-point temperatures and have shown some potential for use in high-temperature structural applications. The fcc $C15$ Laves phases are particularly good candidates for materials applications as they exhibit the best deformation characteristics of the three Laves-phase polytypes. To systematically identify compounds for particular applications, an understanding of their basic elastic properties is required.[21,22] Second, a number of Laves-phase alloys (e.g.,

HfV_2 and ZrV_2) are known to be type-II superconductors with superconducting transition temperatures which are reasonably high for intermetallic materials.[23–27] In some cases[23,28] it was found that the superconducting transition at low temperature was preceded by a structural phase change occuring at higher temperatures (~100 K).

Interestingly, HfV_2 and ZrV_2 also show rather unusual elastic properties, with a number of elastic moduli exhibiting anomalous temperature dependencies. Measurements of the longitudinal-wave sound velocities in polycrystalline HfV_2 and ZrV_2 by Takashima and Hayashi[29] found that the velocities decreased on cooling from room temperature down to ~115 K, but then increased with further cooling. Polycrystalline TaV_2, however, showed only a slight increase in the longitudinal velocity on cooling from room temperature to 4.2 K. Balankin *et al.*[30] measured the temperature dependence of $G(T)$ and $E(T)$ in HfV_2 and ZrV_2. Both compounds showed a V-shaped minimum in $G(T)$ centered at temperatures of ~100 K with an anomalous stiffening with increasing temperature above 100 K up to the vicinity of the melting temperature (~1500 K). A large number of experimental and theoretical studies[29–33] have specifically investigated the possible interrelationship between the anomalous elastic properties, lattice instability, and superconductivity observed in the $C15$ Laves phases.

The elastic properties of TaV_2 have been studied theoretically, and an anomalous temperature dependence was predicted above room temperature.[18] We have recently measured the elastic moduli of polycrystalline TaV_2 down to low temperatures and found that both $G(T)$ and $E(T)$ displayed atypical temperature dependences.[34] Both moduli *increased* with *increasing* temperature over the entire temperature range of 15–300 K. (The bulk modulus was found to increase slightly with *cooling*, in agreement with the sound velocity measurements of Takashima and Hayashi.[29]) Remarkably, it was found that the addition of relatively small amounts of hydrogen or deuterium drastically changed the temperature dependence. The temperature dependences of both $G(T)$ and $E(T)$ for $TaV_2H_{0.34}$, $TaV_2H_{0.53}$, and $TaV_2D_{0.17}$ were reversed over this temperature range, displaying a more typical behavior.[34] The *magnitude* of $G(T)$ was also found to be highly dependent on the H concentration, with a systematic stiffening with increasing H concentration.

The unusual elastic properties of these early-transition-metal $C15$ Laves-phase materials have been attributed to an electronic band-structure effect.[9,23,32,33] (Somewhat similar band-structure effects have been studied in bcc Nb alloys.[35]) The symmetry of the $C15$ lattice allows for a double degeneracy of electronic energy levels at the X point of the irreducible Brillouin zone (IBZ). If the Fermi level of the system lies near the double-degeneracy point, strong effects on the elastic constant may result. For the $C15$ structure, it can be shown[33] that these electronic energy levels couple to the single-crystal elastic constant c_{44}. The effects are rather sensitive to the distance of the Fermi level from the double-degeneracy point. It has been shown that the addition of hydrogen to a metallic material can raise the Fermi level[36,37] by contributing electrons to the conduction band. This interpretation was used to qualitatively account for effects of hydrogen on both the magnitude and temperature dependences of the elastic moduli of $TaV_2H(D)_x$ described briefly above.[34,38]

To explore in more detail the effects of hydrogen on the elastic properties of TaV_2, a mechanical resonance technique has been used to measure the elastic moduli of $TaV_2H(D)_x$ for a series of H(D) concentrations. Preliminary results and analysis have been reported briefly in an earlier work.[38] The present paper reports similar measurements made over an extended temperature range of 3–345 K. Additionally, a number of experimental modifications have significantly improved the quality of the modulus data, permitting a more detailed analysis incorporating the electronic band-structure model. The analysis includes a comparison to electronic density of states measurements from other experiments. Finally, the question of lattice instability and how this relates to the unusual elastic properties of $TaV_2H(D)_x$ is also addressed.

II. EXPERIMENTAL DETAILS

Polycrystalline TaV_2 samples were prepared by arc melting mixtures of the appropriate amounts of the high-purity constituent elements in an argon atmosphere followed by various annealing procedures.[39] Samples of TaV_2H_x were prepared as has been described previously.[39] X-ray diffraction studies have shown that at room temperature all the samples are single-phase solid solutions of hydrogen in TaV_2 with the cubic $C15$-type host-metal structure. In the studied range of hydrogen concentrations, $TaV_2H(D)_x$ samples do not show any phase transitions down to low temperatures.[39]

Ultrasonic measurements were made on samples of $TaV_2H(D)_x$ for $x(H)=0.00$, 0.06, 0.10, 0.18, 0.34, and 0.53 and $x(D)=0.17$. A low-speed diamond saw was used to cut the samples into approximate rectangular parallelepipeds (RP) from button ingots. These saw-cut pieces were then hand polished into accurate RPs with edge dimensions on the order of 1–2 mm. The technique of resonant ultrasound spectroscopy[40–43] (RUS) was used to measure the adiabatic polycrystalline elastic moduli. With RUS, a large number of the lower-frequency mechanical resonances of the RP samples are excited and their frequencies measured. The swept-sine measurements were made using a commercial spectrometer (Dynamic Resonance Systems, Inc.). The elastic constants were determined by performing an iterative computation[44] which minimizes the error between the measured and computed frequencies. In all cases, the frequencies of 40–50 resonances were measured with a typical root-mean-square (rms) difference between the measured and computed frequencies of 0.25%–0.40%. For materials with isotropic symmetry, only two independent moduli are required to fully define the elasticity of the system. The aggregate elastic moduli C_{11} and C_{44} were derived directly from the measured frequencies. C_{44} is just the usual polycrystalline shear modulus $G(T)$. The temperature-dependent measurements below room temperature were made using a commercial ^{4}He cryostat and temperature controller. The measurements were made with the samples in a low-pressure (≈4 mbar) atmosphere of ^{4}He gas. Above room temperature

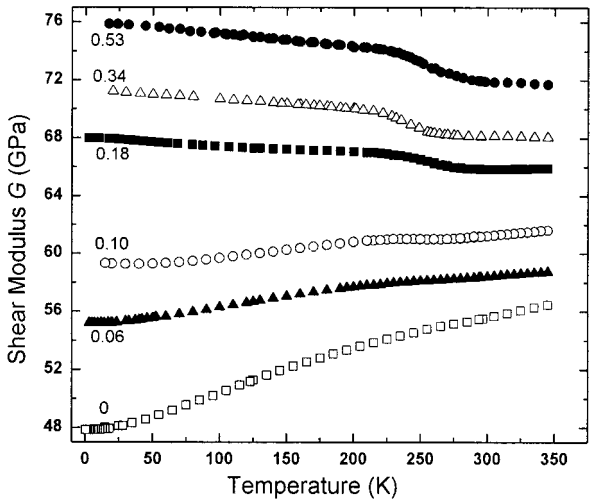

FIG. 1. Elastic shear modulus of polycrystalline TaV_2H_x vs temperature for $x=0.00$, 0.06, 0.10, 0.18, 0.34, and 0.53.

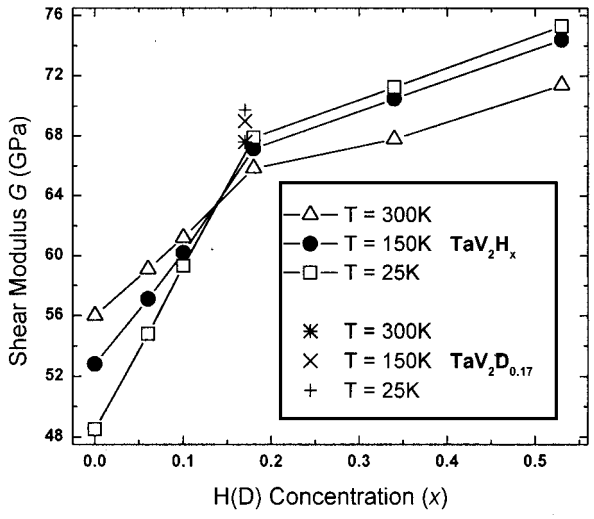

FIG. 2. Elastic shear modulus of polycrystalline TaV_2H_x vs concentration (x) at 25, 150, and 300 K. Data for $TaV_2D_{0.17}$ are also shown.

measurements were made at atmospheric pressure using a commercial oven. The temperature resolution for both experiments was $\approx$0.1 K.

Errors in the mass density result in comparable errors in the absolute values of the elastic moduli derived from the measured resonant frequencies. The room-temperature densities (ρ_M) as determined by direct measurement of the mass and sample dimensions were used. Taking into account both the rms errors in the RUS fit and those estimated for the density measurements, the resulting overall error in the absolute value of G is approximately 1%. The relative error is, of course, much smaller and is essentially indicated by the scatter in the data.

Theoretical densities (ρ_T) were calculated from the experimentally determined room-temperature lattice parameters.[45] As can be seen from Table I, the measured densities are systematically about 4% lower than the theoretical densities for all the $TaV_2H(D)_x$ compounds. It is not surprising that the measured densities may be somewhat lower than those calculated from the x-ray lattice parameters due to the presence of grain boundaries, dislocations, and possible microvoids in the polycrystalline materials. The differences between the two sets of densities, while reasonable, could have some effect on the absolute value of the measured elastic moduli.

Because thermal expansion data are not available for these materials, the results have not been corrected for thermal contraction; the room-temperature dimensions and density have been used in the analysis. Taking into account the direct dimensional effects as well as the indirect effect through the density, the elastic constants deduced from the measured frequencies vary inversely with the dimensions. Metals such as Ta and Zr have a total thermal contraction[46] between room temperature and 4 K of less than 0.20%. Assuming that the materials in the present study behave similarly, neglecting thermal contraction effects in the analysis of the data leads to a comparable error: the total change in the elastic constants as the temperature is lowered from room temperature to 4 K would be roughly 0.15%–0.20% higher than the values reported below.

III. RESULTS AND DISCUSSION

Figure 1 shows the experimentally determined shear modulus of TaV_2H_x, for $x=0.00$, 0.06, 0.10, 0.18, 0.34, and 0.53. It is immediately apparent that the magnitude of the shear modulus of TaV_2H_x systematically increases with increasing hydrogen concentration (x). The effect is greatest at low temperatures, but persists across the entire temperature range. At 20 K the shear modulus of $TaV_2H_{0.53}$ is 55% greater than that of TaV_2. Figure 2 shows the hydrogen concentration dependence of $G(T)$ at three temperatures: 25, 150, and 300 K. Included for comparison in Fig. 2 are data for $TaV_2D_{0.17}$. The shear modulus of TaV_2H_x increases rap-

TABLE I. Experimental densities ρ_M were directly determined from the measured mass and dimensions; theoretical densities ρ_T were calculated from measured lattice parameters.

x	0.00	0.06	0.10	0.17 (D)	0.18	0.34	0.53
ρ_M	9.815	9.828	9.738	9.750	9.751	9.708	9.711
ρ_T	10.25	10.22	10.21	n/a	10.17	10.11	10.03
% diff	−4.23	−3.86	−4.58	n/a	−4.15	−3.96	−3.19

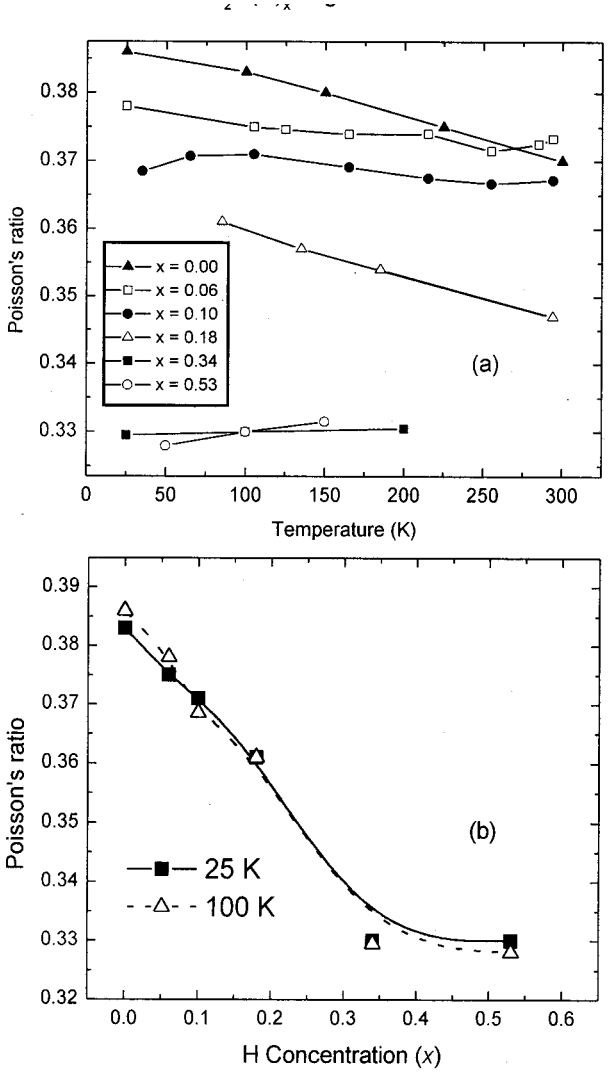

FIG. 3. Poisson's ratio of TaV_2H_x as a function of (a) temperature and (b) H concentration (x). The solid and dashed lines in the figures are guides to the eye.

idly and almost linearly with concentration up to $x=0.18$, after which $G(T)$ continues to increase roughly linearly, but less rapidly, up to $x=0.53$. Poisson's ratio is shown in Fig. 3 both as a function of temperature for the different concentrations and as a function of concentration at two different temperatures. Poisson's ratio is bounded theoretically between 0 and 0.5, although for most materials ν has a value between 0.25 and 0.40. Poisson's ratios of both HfV_2 and ZrV_2 have been measured with an ultrasonic technique and both were found to have a value of 0.37 ± 0.008 at 300 K.[30] It can be seen that TaV_2 has a similar value of $\nu=0.370\pm0.005$ at 300 K, which increases slowly with decreasing temperature. Typical behavior for most materials is that $\nu(T)$ increases with increasing temperature.[3] Figure 3(b) shows the H concentration dependence of ν at two temperatures: 25 and 100 K. It can be observed that ν initially drops almost linearly with increasing concentration until flattening out at a value of 0.33 for $x\geqslant0.34$.

The elastic moduli of $TaV_2H_{0.18}$ and $TaV_2D_{0.17}$ are shown

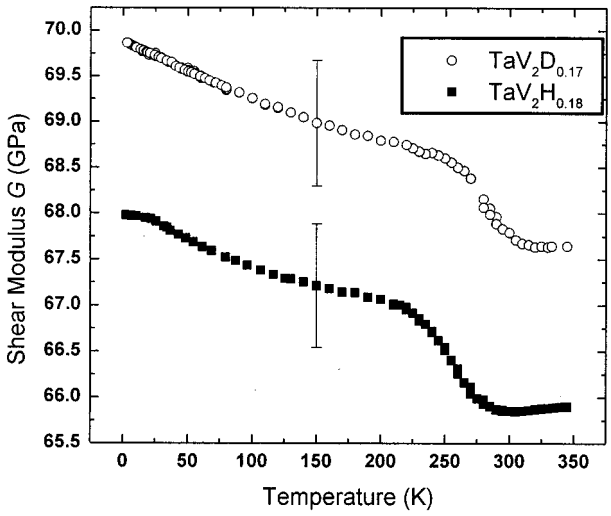

FIG. 4. Elastic shear modulus of polycrystalline $TaV_2H_{0.18}$ and $TaV_2D_{0.17}$ vs temperature. The "steps" observed near 275 K are associated with the motion of hydrogen as discussed in the text.

across the entire temperature range of study in Fig. 4. The error bars indicate that the difference in the shear moduli of $TaV_2H_{0.18}$ and $TaV_2D_{0.17}$ is just outside the range of experimental error. There does not appear to be a significant isotope effect in either the magnitude or the temperature dependence of $G(T)$ except at temperatures below roughly 30 K. Here $G(T)$ of $TaV_2D_{0.17}$ continues to increase almost uniformly down to 3 K, whereas $G(T)$ of $TaV_2H_{0.18}$ begins to flatten out at $\approx$30 K and approaches 3 K with zero slope. It was suggested that this effect is associated with the resonant tunneling of H about g-type interstitial sites within the $C15$ host lattice.[47]

Figure 5 shows $G(T)$ for TaV_2H_x for $x=0.00$, 0.06, and 0.10 on an expanded scale and highlights the anomalous temperature dependence of $G(T)$ displayed by these concentrations. For TaV_2 the modulus decreases with decreasing temperature from 345 K until $\sim$10 K where it begins to flatten out. Below 10 K, $G(T)$ is almost temperature independent and approaches 0.3 K with zero slope. (Measurements for TaV_2 were carried out down to 0.3 K; in general, the measurements only extended down to 3 K.) The modulus for $TaV_2H_{0.06}$ shows a similar softening with decreasing temperature, but with a somewhat weaker temperature dependence. $TaV_2H_{0.10}$ also shows a softening with decreasing temperature down to $\sim$40 K, but then a stiffening as the temperature is decreased further to 15 K. This shallow minimum in the shear modulus of $TaV_2H_{0.10}$ can be seen on the expanded-scale inset in Fig. 5. This minimum will be a key parameter in the analysis presented below.

As Figs. 1 and 5 show, the temperature dependence of $G(T)$ for H(D) concentrations $x\geqslant0.17$ is reversed from that of the lower concentrations. Furthermore, a "step" in $G(T)$ is clearly visible for all higher concentrations ($x\geqslant0.17$) in the temperature range of 225–300 K. Such steps were observed for all $x>0.00$, but are too small to be seen in Fig. 1 for $x\leqslant0.10$. This effect is associated with the motion of hy-

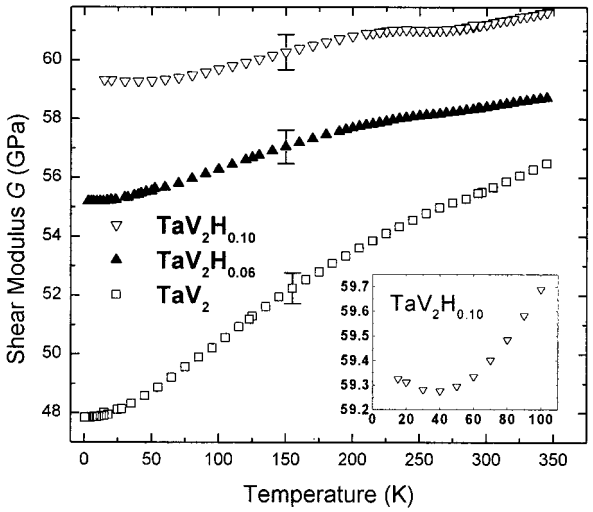

FIG. 5. An expanded view of the data shown in Fig. 1 for $x=0.00$, 0.06, and 0.10. The inset shows a minimum in $G(T)$ for $x=0.10$ at approximately 40 K.

drogen in these materials.[48,49] The present ultrasonic measurements were made in the frequency range of 0.4–2.0 MHz. The condition $\omega\tau\approx 1$ is satisfied, in these compounds at approximately 260 K, where ω is the angular frequency of the ultrasound and τ is the characteristic relaxation time of the hydrogen. In the present case τ is the time for hydrogen to respond to an external stress by hopping among interstitial sites. The data below roughly 225 K represent the unrelaxed elastic modulus, while the data above 300 K represent the relaxed elastic modulus. More precisely, the lower-temperature data represent the adiabatic, unrelaxed modulus, while the higher-temperature represent the adiabatic, relaxed modulus.

Associated with the shift in $G(T)$, large ultrasonic loss peaks were observed for all $x>0.00$ in the temperature range of 225–300 K. The ultrasonic loss peaks arise as a result of the relaxation of H atoms under the applied strain. A full description of the attenuation measurements and the motion of hydrogen in these materials have been reported[48,49] previously, but the major points will be discussed briefly. The ultrasonic loss peaks were fit using a Debye-type expression for the ultrasonic loss, $1/Q$, given by

$$\frac{1}{Q}=\left(\frac{\Delta c}{c}\right)\frac{\omega\tau}{1+\omega^2\tau^2}, \tag{1}$$

where Q is the quality factor of the resonant line shapes, $(\Delta c/c)$ is usually referred to as the relaxation strength, c is an elastic constant, and $\Delta c=c_U-c_R$, where c_U and c_R are the unrelaxed and relaxed moduli, respectively. In most cases a simple Arrenhius expression was used for the relaxation time

$$\tau=\tau_0\exp(E_A/k_BT). \tag{2}$$

The parameters obtained from these fits included the relaxation strength, activation energies (E_A), and attempt frequencies (τ_0^{-1}). The temperature-dependent shift in the elastic constants, δc, is given by[50]

$$\delta c=\Delta c\,\frac{\omega^2\tau^2}{1+\omega^2\tau^2}. \tag{3}$$

It was shown[49] that the shift in $G(T)$ for all H concentrations could be accounted for using the same parameters derived from the ultrasonic loss measurements. The purpose of the present study is to examine possible electronic effects on the temperature dependence of $G(T)$, unrelated to the hydrogen motion. Therefore, as the magnitude and temperature dependence of the relaxation effects on $G(T)$ were successfully described using parameters from the loss measurements, this contribution has been removed from the $G(T)$ data of Fig. 1. The relaxation-corrected data are presented in Fig. 6(a). The underlying temperature dependence of $G(T)$ is now evident. The relaxation correction for $G(T)$ was not made for the lower concentrations, $x\leqslant 0.10$, where the effect was small. The relaxation-corrected modulus for $TaV_2H_{0.18}$ shows a weak minimum at roughly 300 K, although it is too shallow to be seen in Fig. 6(a). No such minimum is seen for the $x=0.34$ and 0.53 concentrations or indeed for the deuterated sample, although the form of the data in Fig. 6(a) strongly suggests that the moduli are approaching minima at higher temperatures.

The results are interpreted in terms of the unusual electronic structure effects[9,23,32,33] proposed for the $C15$ materials, which were discussed briefly in the Introduction. The $C15$ symmetry allows for doubly degenerate electronic levels at the X point of the IBZ with a linear dispersion relation in the vicinity of this point. The degeneracy and linear dispersion have been confirmed by band-structure calculations.[9] From symmetry considerations these levels couple to a strain e_4.[33] A key parameter in the model concerns the position of the Fermi level with respect to this double-degeneracy point; if the Fermi level is near this point, then these bands contribute strongly to the temperature dependence of the corresponding single-crystal elastic constant c_{44}. The arguments are outlined further below. The Helmholtz free energy of a system of N electrons each of energy ξ_{bk} is given by

$$F=N\xi_F-2\sum_{bk}\,k_BT\ln\left[1+\exp\frac{\xi_F-\xi_{bk}}{k_BT}\right], \tag{4}$$

where ξ_F is the Fermi energy, the sum is over all energy bands b and all k values, and the factor 2 accounts for spin. We consider only the doubly degenerate levels in the vicinity of the X point and express these levels as[33]

$$\xi_{1,2}(k)=\pm\sqrt{(sk)^2+(\gamma e_4)^2}, \tag{5}$$

where ξ_F, $\xi_{1,2}$, and k, the electron wave number, are measured with respect to the doubly degenerate point, s is a proportionality constant, and γ is the deformation potential. Using $c_{44}^e=\partial^2F/\partial e_4^2$ gives, in the present case, the simple result

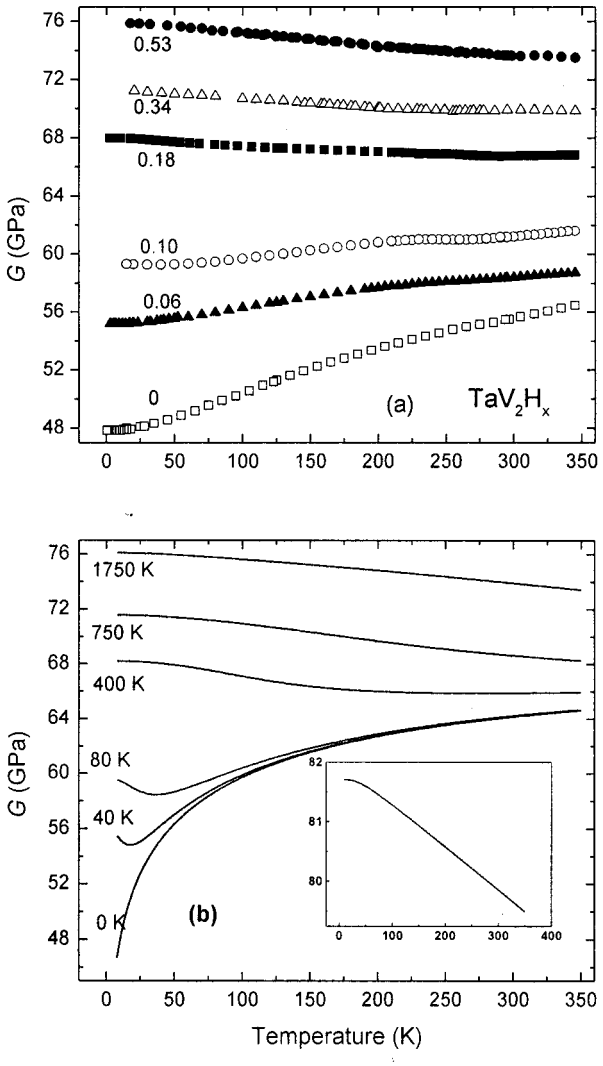

FIG. 6. Elastic shear modulus of polycrystalline TaV_2H_x vs temperature for $x=0.00$, 0.06, 0.10, 0.18, 0.34, and 0.53. (a) Experimental data. The results for $x \geqslant 0.18$ have been corrected for the effect of the H relaxation on $G(T)$ as discussed in the text. (b) Calculated values of $G(T)$ vs x. The "background" elastic constant used in the calculation is shown in the inset. The values of the Fermi energies used in the calculation are listed in units of kelvin and were derived from Fig. 7.

$$c_{44} = \pm 2\gamma^2 \sum_k \frac{f(k_z)}{sk_z}, \tag{6}$$

where $f(k_z)$ is the Fermi-Dirac distribution function. Setting $\varepsilon = sk_z$, expressing the exponentials in terms of hyperbolic functions, and converting the sum to an integral results in[9,18,33,34]

$$c_{44}^e \propto -\gamma^2 \int_0^\Omega \frac{d\varepsilon}{\varepsilon}\left[\frac{\sinh(\varepsilon/k_BT)}{\cosh(\varepsilon/k_BT)+\cosh(\xi_F/k_BT)}\right], \tag{7}$$

where the qualitative features are not strongly dependent on the range of integration, Ω. The band-structure calculation[9] indicates that $\Omega = 5000$ K represents a reasonable range for the linear dispersion, and this value will be used below. It can be seen from Eq. (6) that those electrons filling the lower energy band provide a negative contribution to c_{44}.

It was shown previously[34,38] that Eq. (7) accounts qualitatively for the x and T dependence of the shear modulus. Using the more extensive data shown in Fig. 1 and correcting for the effects of dispersion as indicated in Fig. 6(a), a more detailed comparison of the data to the theoretical model is presented in the following discussion. The model and data indicate that the Fermi level for the $x=0$ case lies very near the double-degeneracy point. To be specific for the calculation, we assume that the Fermi level for this case passes through the double-degeneracy point: i.e., we take $\xi_F = 0$ for $x=0$. Figure 5 shows a clear minimum in $G(T)$ for $x=0.10$. In terms of the model, this minimum indicates that $\xi_F \approx 80$ K for $x=0.10$. We now proceed to calculate the shear modulus $G(T)$ using

$$G(T,x) = C_{\rm bg}(T) - K\int_0^\Omega \frac{d\varepsilon}{\varepsilon}\left[\frac{\sinh(\varepsilon/k_BT)}{\cosh(\varepsilon/k_BT)+\cosh(\xi_F/k_BT)}\right], \tag{8}$$

where $C_{\rm bg}(T)$ is a background term representing all the other contributions to the elastic constants such as the ion-core, phonon, and other electronic contributions. The constant K is proportional to γ^2, but also includes other factors which are difficult to quantify. There is a phase-space volume contribution[33] and a factor to account for the fact that the model is for the single-crystal elastic constant c_{44}. It should be remembered that the measurements are for the aggregate elastic constant $G = C_{44}$, which will have contributions from the other single-crystal elastic constants. K will be found by fitting the data. First, we calculate $G(T)$ as a function of the Fermi energy at 10 K to determine fitting constants. We choose this temperature because the effects of the electronic structure model are largest at low temperatures. Other effects not associated with the model will be relatively less important, and more reliable fitting constants may be found. At this temperature we take $C_{\rm bg} = C_0$. To determine the two constants C_0 and K we set two conditions: (i) for $x=0$, we take $\xi_F = 0$ and $G(10\ {\rm K}) = 47.8$ GPa, and (ii) for $x=0.10$, we take $\xi_F = 80$ K and $G(10\ {\rm K}) = 59.5$ GPa. These Fermi energies were chosen because $G(T)$ for $x=0$ increases with temperature throughout the temperature range investigated and $G(T)$ for $x=0.10$ shows a clear minimum at about 40 K. The values of G are the experimental values at 10 K for these two x values. Putting these two conditions into Eq. (8) gives $C_0 = 81.7$ GPa and $K = 5.34$ GPa. The result of the calculation of G vs ξ_F with these two constants is shown in Fig. 7. Using Fig. 7, we now determine the Fermi energies for the other four x values by projecting the $G(10\ {\rm K})$ values for each concentration onto the ξ_F axis. This process is indicated by the dashed lines in Fig. 7.

With C_0, K, and the Fermi energies determined, we now use Eq. (8) to calculate the full temperature and x dependence of G. To estimate the temperature dependence of the background term we use the convenient Varshni expression[3]

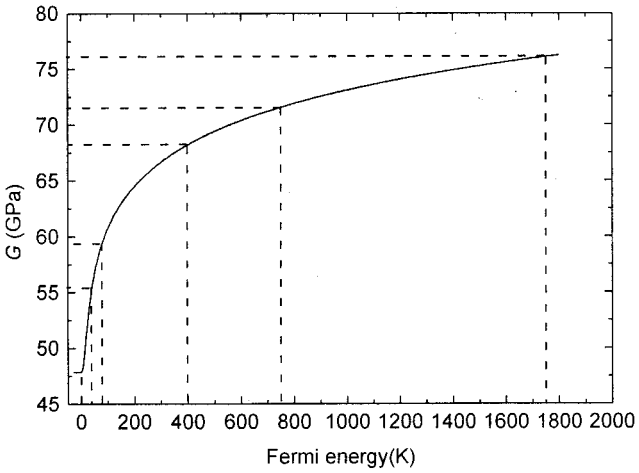

FIG. 7. Calculated values of the elastic shear modulus vs Fermi energy at 10 K from Eq. (8). The constants C_0 and K used in the calculation are listed in the text. The curve was constrained to pass through the two points (47.8 GPa, 0 K) and (59.5 GPa, 80 K) as discussed in the text. The dashed lines indicated the projection of the experimental values of the 10-K elastic constants onto the Fermi energy axis to determine ξ_F for $x=0.06$, 0.18, 0.34, and 0.53. These values of ξ_F were used for the computation of Fig. 6(b).

$$C_{\mathrm{bg}}(T)=C_0-\frac{s}{\exp(t/T)-1}, \tag{9}$$

with $s=0.73$ GPa and $t=100$ K. These values of s and t were estimated from $G(T=350\ \mathrm{K},\ x=0.53)$. The resulting temperature dependence of C_{bg} is comparable to that found experimentally[34] for $ZrCr_2$, a $C15$ Laves-phase compound which does not show the unusual temperature dependence of TaV_2. It should be emphasized that the conclusions would not be changed significantly if the temperature dependence of C_{bg} were neglected altogether. The results of the calculation of $G(x,T)$ are shown in Fig. 6(b). The background elastic constant is indicated in the inset of Fig. 6(b). Comparing Figs. 6(a) and 6(b), it can be seen that this simple model accounts for the major features of the data.

There are a number of possible contributions to the elastic constants which are not taken into account in the present analysis and which may contribute to the differences between the measured and computed values of $G(T)$. Because the lattice expands with the addition of hydrogen, the background elastic constant may depend on hydrogen concentration. We have used the same C_{bg} for all x. In terms of the model used, the constant γ could be k dependent. In addition, there may be other electron and phonon contributions which could be x dependent and which are not included in the model. There are basically four parameters in the model: C_0, K, and the values of the Fermi energies for the two concentrations 0.00 and 0.10. The parameters s and t have only a minor effect.

We now turn to a discussion of the shift of the Fermi level with the addition of hydrogen. The general idea is that each hydrogen atom will contribute a fraction of an electron to the conduction band. These electrons will raise the Fermi level. An important parameter is the density of states at the Fermi level, $N(\xi_F)$. A large $N(\xi_F)$ will mean a small shift and vice versa. Figure 8 gives the shift of ξ_{F} vs x as determined from Fig. 7 for the six x values of the present work (solid points in the plot). The fact that the plot turns upward as a function of x indicates that $N(\xi_F)$ decreases with increasing x. Fortunately, there is experimental information about $N(\xi_F)$ for TaV_2H_x from nuclear magnetic resonance (NMR) experiments.[51] The NMR results indeed show that $N(\xi_F)$ initially decreases with the addition of hydrogen, levels off above $x=0.56$ and passes through a minimum at $x=0.8$.

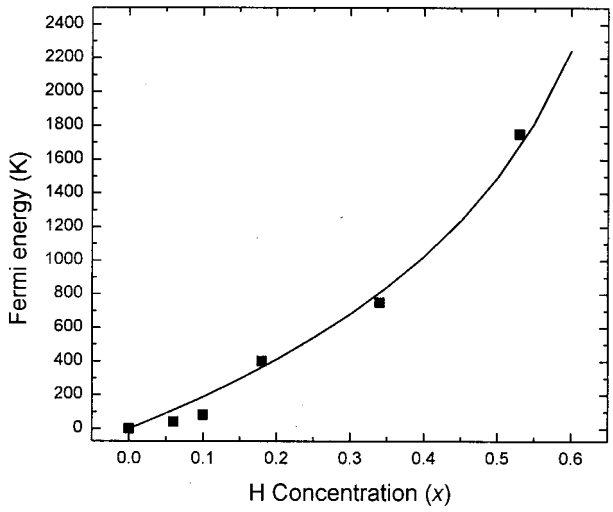

FIG. 8. Shift of the Fermi energy vs H concentration (x). The points were determined from the elastic constant measurements. The solid line was computed from density of states results with the assumption that each H atom contributes one electron at the Fermi level.

The comparison can be made more quantitative. The shift of the Fermi energy, $\Delta\xi_F$, is related to the increase in hydrogen concentration, Δx, by $N(\xi_F,x)\Delta\xi_F=f\Delta x$, where f is the fraction of an electron each added hydrogen atom contributes at the Fermi level. The Fermi energy at x relative to the value at zero hydrogen concentration is then given by

$$\xi_F=\int_0^x \frac{f\,dx'}{N(\xi_F,x')}. \tag{10}$$

The NMR results are available for three x values—0.00, 0.22, and 0.56—over the range of the present experiments. Considering just these three points, $N(\xi_F)$ appears to decrease linearly and can be represented by $N(\xi_F,x)=(6.54-9.06x)/(\mathrm{eV\ TaV_2\ unit})$, where a factor of 2 has been included for spin. Using this expression for $N(\xi_F)$ in Eq. (10) gives $\xi_F=-0.11f\ln(1-1.38x)$ eV. This expression is represented by the solid line in Fig. 8 for $f=1$. It can be seen that this expression fits the data remarkably well. This implies that each hydrogen atom contributes an electron at the Fermi level. Although electronic structure calculations are not available for TaV_2H_x, calculations for other systems[36]

show that f ranges from 0.5 for PdH to 1.0 for CrH. However, the value $f \approx 1$ is expected for a dilute hydrogen-metal system where hydrogen-hydrogen interactions can be neglected.[36] In the present case, even at $x = 0.53$ only about 4% of g sites are occupied, so the system may be considered dilute. In addition, ultrasonic attenuation measurements[49] show that the loss peak due to hydrogen motion is linear in the hydrogen concentration (Snoek effect) which is additional support for the relative unimportance of hydrogen-hydrogen interactions. The agreement between the two sets of shifts in Fig. 8 is striking and provides strong support for the model of electronic-structure-induced changes in the elastic shear modulus. The discrepancy between elastic-constant-derived shifts and those computed from the density of states (DOS) in the range $0 \leqslant x \leqslant 0.1$ could be accounted for by a higher DOS in this range; the NMR measurements did not provide details about $N(\xi_F)$ in this range and the linear interpolation may not represent the actual situation.

Now the question of lattice instability in $C15$ Laves phases and the relationship to the observed anomalous elastic properties will be addressed. There is evidence from a series of experimental studies that a structural phase transition occurs at roughly 100 K in cubic HfV_2 and ZrV_2.[30,32,52–55] The first-order structural phase transition appears to be preceded by an electronic transition at 125 and 160 K for HfV_2 and ZrV_2, respectively.[30] It is within this temperature range at which unusual effects were observed for Poisson's ratio, $G(T)$, $E(T)$, and $B(T)$ in these systems. The evidence suggests that the low-temperature phase of HfV_2 is either tetragonal or orthorhombic and that of ZrV_2 is either rhombohedral[56] or orthorhombic.[23] The symmetry of the low-temperature phases has not been determined conclusively and appears to be sensitive to the impurity content in the material.[57]

The electronic model described above has been used to account for the anomalous elastic properties in the HfV_2 and ZrV_2 systems. Izyumov *et al.*[33] suggested that the total softening of c_{44} due to the cancellation of the positive normal ionic contribution (c_{44}^i) by the negative electronic contribution (c_{44}^e) was directly responsible for the lattice instability. It is known that the anomalies in specific heat and resistivity measurements observed for HfV_2 can be removed by the addition of small quantities of Nb (3%–5%), stabilizing the cubic high-temperature phase.[32] It was also found that HfV_2 doped with 15 at. % Nb did *not* show a specific heat anomaly, but *did* exhibit similar unusual elastic properties.[32] This observation provided initial evidence for the arguments made by Chu *et al.* that the softening of c_{44}^e may not be the underlying mechanism for the lattice instability.[32] Chu *et al.*[32] used first-principles calculations to determine the total energy and electronic structure of $C15$ MV_2 (M = Ta, Hf, and Zr) and estimated that the Fermi level of HfV_2 and ZrV_2 lies roughly 800 K above the double-degeneracy point. For this value of the Fermi level the model implies that the c_{44}^e contribution would stiffen with decreasing temperature below $\approx$350 K. Therefore, it was argued that the low-temperature phase transformation could not be caused by the cancellation of c_{44}^i by c_{44}^e. Instead, it was proposed that the lattice instability in HfV_2 and ZrV_2 was related to the high value of the DOS at the Fermi level $[N(\xi_F)]$ and to the geometry of the Fermi surface.[32]

A number of theoretical studies have confirmed the presence of a large, narrow peak in the DOS of HfV_2 and ZrV_2 and that the Fermi level lies on this peak.[32,58,59] A large $N(\xi_F)$ and a sharp peak in the DOS can result in a strong electron-phonon coupling. The physical effect of this coupling is dependent on the specific geometry of the Fermi surface. In the case of HfV_2 and ZrV_2 it was argued that Fermi surface nesting results in an incommensurate electronic charge density wave along the $\langle 100 \rangle$ direction. It was argued that the combination of the high electron-phonon coupling and the charge-density wave induced by Fermi surface nesting could cause the displacement of atoms at lower temperatures, leading to phonon softening, lattice instability, and the phase transition.[32]

Similar experimental studies[32,55] performed on TaV_2 have not shown any evidence for a phase transition: TaV_2 maintains the cubic $C15$ structure down to at least 4 K. Data for $B(T)$, $E(T)$, and Poisson's ratio previously reported[34] and the data reported here for $G(T)$ and Poisson's ratio show no discontinuities or inflection points throughout the temperature range studied. The lack of a phase transition in TaV_2 was rationalized by Chu *et al.*[32] who showed that TaV_2, having one more d electron per formula unit has an increased Fermi energy, resulting in both a reduction in $N(\xi_F)$ (as the Fermi level shifts away from the DOS peak) and the disappearance of the Fermi surface nesting. As in the Hf-Nb-V system for $>5\%$ Nb, the TaV_2 alloy displays anomalous elastic properties, but without an associated structural phase transition.[32]

However, as the electronic model implies, our results for C_{44} indicate that the Fermi level of TaV_2 appears to be very close to the double-degeneracy level at the X point of the IBZ in contradiction to the band-structure calculations.[32] It is interesting to note that if the calculated Fermi levels of HfV_2, ZrV_2, and TaV_2 are systematically lowered so that the ξ_F of TaV_2 is roughly 0 K above the X point, then the ξ_F of HfV_2 and ZrV_2 would lie $\sim$200 K below the X point. For this value of ξ_F the electronic model would predict a softening of c_{44} for HfV_2 and ZrV_2 down to $\sim$100 K, as observed. It seems reasonable that the negative electronic contribution to c_{44} may persist below room temperature and contribute to the lattice instability of HfV_2 and ZrV_2.

IV. CONCLUSIONS

Measurements of the elastic shear modulus of polycrystalline $TaV_2H(D)_x$ over a temperature range of 3–345 K have revealed several striking features. Both the temperature dependence and magnitude of the shear modulus are highly dependent on the hydrogen concentration. At 20 K, $G(T)$ for $TaV_2H_{0.53}$ is 55% stiffer than that of TaV_2. For H concentrations $x \leqslant 0.10$, $G(T)$ shows anomalous stiffening with increasing temperature almost across the entire temperature range of study. $TaV_2H_{0.10}$ displays a minimum in $G(T)$ at roughly 40 K. For H concentrations $x \geqslant 0.18$ the temperature dependence of $G(T)$ is reversed compared to that of the

lower concentrations and exhibits softening with increasing temperature. Comparison of the results for $TaV_2H_{0.18}$ and $TaV_2D_{0.17}$ indicates that there is not a strong isotope effect on $G(T)$.

The results are in agreement with a model detailing electronic contributions to the single-crystal elastic constant c_{44}. The symmetry of the $C15$ structure results in doubly degenerate electronic energy levels at the X point of the Brillouin zone. These levels couple to an e_4 strain with resulting effects on the single-crystal elastic constant c_{44}, thereby modifying the shear modulus $G(T)$ of the polycrystalline samples. Hydrogen donates electrons to the conduction band and thus shifts the Fermi level above the double-degeneracy point. As a result, the electronic contributions to c_{44} are strongly affected. The shift of the Fermi energy as a function of the hydrogen concentration x determined from the elastic constant measurements is in remarkable agreement with the shift predicted from electronic density of states data available from nuclear magnetic resonance experiments. The present results indicate that each hydrogen atom contributes approximately one electron at the Fermi level.

ACKNOWLEDGMENTS

The work at Colorado State University was supported by the U.S. National Science Foundation under Grant No. DMR-0070808. The work at the Institute of Metal Physics in Ekaterinburg was partially supported by the Russian Foundation for Basic Research (Grant No. 99-02-16311).

[1] J. F. Nye, *Physical Properties of Crystals* (Clarendon, Oxford, 1957).
[2] D. C. Wallace, Phys. Rev. **162**, B776 (1967).
[3] H. M. Ledbetter, in *Materials at Low Temperatures*, edited by R. P. Reed and A. F. Clark (American Society for Metals, Metals Park, OH, 1983), p. 1.
[4] J. A. Garber and A. V. Granatao, Phys. Rev. B **11**, 3990 (1975).
[5] G. A. Alers, in *Physical Acoustics* edited by W. P. Mason (Academic, New York, 1966), Vol. IV, pt. A.
[6] W. L. Rehwald, Adv. Phys. **22**, 721 (1973).
[7] F. Willis and R. G. Leisure, Phys. Rev. B **54**, 9077 (1996).
[8] C. Weinmann and S. Steinemann, Solid State Commun. **15**, 281 (1974).
[9] F. Chu, M. Šob, R. Siegl, T. E. Mitchell, D. P. Pope, and S. P. Chen, Philos. Mag. B **70**, 881 (1994).
[10] H. Anton and P. C. Schmidt, Intermetallics **5**, 449 (1997).
[11] S. Hong and C. L. Fu, Intermetallics **7**, 5 (1999).
[12] G. W. Shannette and J. F. Smith, J. Appl. Phys. **40**, 79 (1969).
[13] R. J. Schlitz and J. F. Smith, J. Appl. Phys. **45**, 4681 (1974).
[14] R. L. Fleischer, R. S. Gilmore, and R. J. Zabala, Acta Metall. **37**, 2801 (1989).
[15] F. Willis, R. G. Leisure, and I. Jacob, Phys. Rev. B **50**, 13 792 (1994).
[16] S. Hong, C. L. Fu, and M. H. Yoo, Intermetallics **7**, 1169 (1999).
[17] B. Wolf, C. Hinkel, S. Holtmeier, D. Wichert, I. Kouroudis, G. Bruls, B. Luthi, M. Hedo, Y. Inada, E. Yamamoto, Y. Haga, and Y. Onuki, J. Low Temp. Phys. **107**, 421 (1997).
[18] F. Chu, M. Lei, A. Migliori, S. P. Chen, and T. E. Mitchell, Philos. Mag. B **70**, 867 (1994).
[19] J. D. Livingston, in *Heat Temperature Silicide and Refractory Alloys*, edited by C. L. Briant, J. J. Petrovic, B. P. Bewlay, A. K. Vasudevan, and H. A. Lipsett, MRS Symposia Proceedings No. 322 (Materials Research Society, Pittsburgh, 1994), p. 395.,
[20] T. E. Mitchell, R. G. Castro, J. J. Petrovic, S. A. Maloy, O. Unal, and M. M. Chadwick, Mater. Sci. Eng., A **155**, 24 (1992).
[21] D. Pope and F. Chu, in *Proceedings of the International Symposium on Structural Intermetallics*, edited by R. Darolia, J. J. Lewandowski, C. T. Liu, P. L. Martin, D. B. Miracle, and M. V. Nathal (Metallurgical Society of AIME, Warrendale, PA, 1993), p. 637.
[22] S. P. Chen, A. F. Voter, R. C. Albers, A. M. Boring, and P. J. Hay, J. Mater. Res. **5**, 955 (1990).
[23] S. V. Vonsovskiy, Yu. A. Izyumov, and E. Z. Kurmayev, *Superconductivity of Transition Metals* (Springer, Berlin, 1982).
[24] A. C. Lawson, Phys. Lett. **38A**, 379 (1972).
[25] K. Inoue, K. Tachskawa, and V. Iwasa, Appl. Phys. Lett. **18**, 235 (1971).
[26] Ö. Rapp and L. J. Vieland, Phys. Lett. **36A**, 369 (1971).
[27] J. Crangle, K. Neumann, and K. Ziebeck, J. Phys. D **29**, 2362 (1996).
[28] V. V. Nemoshkolenko, V. Ya. Nagornyy, and M. T. Kogut, Metallofizika (Kiev) **3**, 29 (1981).
[29] T. Takashima and H. Hayashi, Jpn. J. Appl. Phys., Part 1 **12**, 1659 (1973).
[30] A. S. Balankin, Yu. F. Bychkov, and Ye. I. Yakovlev, Fiz. Met. Metalloved. **56**, 119 (1983).
[31] A. Ormeci, F. Chu, J. M. Wills, T. E. Mitchell, R. C. Albers, D. J. Thoma, and S. P. Chen, Phys. Rev. B **54**, 12 753 (1996).
[32] F. Chu, D. J. Thoma, T. E. Mitchell, C. L. Lin, and M. Šob, Philos. Mag. B **77**, 121 (1998).
[33] Yu. A. Izyumov, V. Ye. Naysh, and V. N. Syromyatnikov, Fiz. Met. Metalloved. **39**, 455 (1975).
[34] K. Foster, J. E. Hightower, R. G. Leisure, and A. V. Skripov, Philos. Mag. B **80**, 1667 (2000).
[35] P. Bujard, R. Sanjines, E. Walker, J. Ashkenazi, and M. Peter, J. Phys. F: Met. Phys. **11**, 775 (1987).
[36] A. C. Switendick, in *Hydrogen in Metals I*, edited by G. Alefeld and J. Volkl, Topics in Applied Physics, Vol. 28 (Springer, Berlin, 1978), p. 101.
[37] Y. Fukai, *The Metal-Hydrogen System* (Springer-Verlag, Berlin, 1993), p. 300.
[38] R. G. Leisure, K. Foster, J. E. Hightower, A. Ode, and A. V. Skripov, J. Alloys Compd. **330–332**, 396 (2002).
[39] A. V. Skripov, M. Yu. Belyaev, S. V. Rychkova, and A. P. Stepanov, J. Phys.: Condens. Matter **1**, 2121 (1989).
[40] I. Ohno, J. Phys. Earth **24**, 355 (1976).
[41] A. Migliori, J. L. Sarrao, W. M. Visscher, T. M. Bell, L. Ming, Z. Fisk, and R. G. Leisure, Physica B **183**, 1 (1993).
[42] A. Migliori and J. L. Sarrao, *Resonant Ultrasound Spectroscopy* (Wiley, New York, 1997).

[43] R. G. Leisure and F. A. Willis, J. Phys.: Condens. Matter **9**, 6001 (1997).
[44] W. M. Visscher, A. Migliori, T. M. Bell, and R. A. Reinert, J. Acoust. Soc. Am. **90**, 2154 (1991).
[45] A. V. Skripov and V. N. Kozhanov (unpublished).
[46] G. K. White, *Experimental Techniques in Low Temperature Physics* (Oxford University Press, New York, 1968), p. 285.
[47] K. Foster, R. G. Leisure, and A. V. Skripov, Phys. Rev. B **64**, 214302 (2001).
[48] K. Foster, R. G. Leisure, and A. V. Skripov, J. Phys.: Condens. Matter **11**, 799 (1999).
[49] K. Foster, R. G. Leisure, J. E. Hightower, and A. V. Skripov, J. Phys.: Condens. Matter **13**, 7327 (2001).
[50] R. G. Leisure, in *Resonant Ultrasound Spectroscopy*, edited by A. Migliori and J. L. Sarrao (Wiley, New York, 1997), p. 139.
[51] A. V. Skripov, M. Yu. Belyaev, K. N. Mikhalev, and A. P. Stepanov, J. Alloys Compd. **177**, 63 (1991).
[52] A. C. Lawson and W. H. Zachariasen, Phys. Lett. **38A**, 1 (1965).
[53] T. R. Finlayson, E. J. Lanston, M. A. Simpson, E. E. Gibbs, and T. F. Smith, J. Phys. F: Met. Phys. **8**, 2269 (1978).
[54] J. W. Hafstrom, G. S. Knapp, and A. T. Aldred, Phys. Rev. B **17**, 2892 (1978).
[55] A. S. Balankin and D. M. Skorov, Sov. Phys. Solid State **24**, 681 (1982).
[56] V. A. Finkel and Ye. A. Pushkarev, Zh. Eksp. Teor. Fiz. **78**, 842 (1980).
[57] A. S. Balankin, Sov. Phys. Solid State **24**, 2102 (1982).
[58] T. Jarlborg and A. J. Freeman, Phys. Rev. B **22**, 2332 (1980).
[59] A. Ormeci, F. Chu, J. M. Willis, T. E. Mitchell, R. C. Albers, D. J. Thoma, and S. P. Chen, Phys. Rev. B **54**, 12 753 (1996).